ELSEVIER

International Journal of Heat and Fluid Flow 20 (1999) 48–59

International Journal of
HEAT AND FLUID FLOW

Transient response of protruding electronic modules exposed to horizontal cross flow

Muhammad M. Rahman *, Jagannath Raghavan [1]

Department of Mechanical Engineering, University of South Florida, Tampa, FL 33620-5350, USA

Received 25 November 1997; accepted 30 April 1998

Abstract

The objective of this research was to carry out a numerical simulation of heat transfer during cross-flow mixed convection in electronic circuit boards. A buoyancy-driven transport in the vertical direction and a forced convective flow in the horizontal direction results in a three dimensional boundary layer structure adjacent to the board surface. The rate of heat transfer is determined by a combined influence of these two transport processes. It was attempted to identify and analyze the significance of different factors that influence the local heat transfer rate and the temperature of these components and their behavior with change in time. A three-dimensional numerical model of a conducting board of finite thickness with four heat sources mounted on its surface was analysed. Heat transfer from both sides of the board was taken into account. The equations for the conservation of mass, momentum, and energy were solved in the fluid region. In the solid region, the energy equation reduced to the transient heat conduction equation. The solution was carried out simultaneously in the solid and the fluid regions taking into account the continuity of temperature and heat flux at the solid–fluid interfaces. The important parameters that influenced the heat transfer mechanism were the distance of the heat sources from the natural as well as the forced convection leading edges, spacing between the sources, board thickness, Richardson number, Reynolds number, and Fourier number. The variation of velocity and temperature fields as well as the Nusselt number with Fourier number for different values of Richardson number were explored. © 1999 Elsevier Science Inc. All rights reserved.

Keywords: Mixed convection; Electronics cooling; Protruding module; Thermal transient

Notation

- b thickness of the board (m)
- B non-dimensional thickness of the board, b/l
- d_y source spacing in the y-direction (m)
- D_y non-dimensional source spacing in the y-direction, d_y/l
- d_z source spacing in the z-direction (m)
- D_z non-dimensional source spacing in the z-direction, d_z/l
- g acceleration due to gravity (m/s^2)
- Gr Grashof number, $g\beta q l^4/k\nu_f^2$
- h heat transfer coefficient (W/m^{2}K)
- h_m thickness of mounted heat source (m)
- H_m non-dimensional thickness of mounted heat source, h_m/l
- k thermal conductivity (W/mK)
- l length or height of heat source (m)
- l_y distance of heat sources from the y-direction leading edge (m)
- L_y non-dimensional heat source distance from the y-direction leading edge (m)
- l_z distance of heat sources from the z-direction leading edge (m)
- L_z non-dimensional heat source distance from the z-direction leading edge (m)
- Nu Nusselt number, hl/k_f
- Pr Prandtl number, ν_f/α_f
- q heat dissipation rate (W/m^2)
- Re Reynolds number, $w_\infty l/\nu_f$
- Ri Richardson number, Gr/Re^2
- T temperature (K)
- u velocity component in the x-direction (m/s)
- U dimensionless velocity component in the x-direction, u/w_∞
- v velocity component in the y-direction (m/s)
- V dimensionless velocity component in the y-direction, v/w_∞
- w velocity component in the z-direction (m/s)
- W dimensionless velocity component in the z-direction, w/w_∞
- x normal coordinate (m)
- X dimensionless normal coordinate, x/l
- y vertical coordinate (m)
- Y dimensionless vertical coordinate, y/l
- z horizontal coordinate (m)
- Z dimensionless horizontal coordinate, z/l

* Corresponding author. E-mail: rahman@eng.usf.edu.

[1] Present Address: CFD Research Corporation, Huntsville, AL 35805, USA

0142-727X/99/$ – see front matter © 1999 Elsevier Science Inc. All rights reserved.
PII: S 0 1 4 2 - 7 2 7 X (9 8) 1 0 0 3 1 - 0

Greek

α thermal diffusivity (m^2/s)
β coefficient of thermal expansion (1/K)
θ dimensionless temperature, $(T - T_\infty)/(ql/k_f)$
ν kinematic viscosity (m^2/s)
τ Fourier number (dimensionless time), $t\alpha_f/l^2$

Subscripts

f fluid
s solid
∞ free stream condition
m mounted module

1. Introduction

Heat transfer has been a challenging subject for designers of electronic equipment. The reliability of an electronic component depends on its operating temperature and its life can be improved very significantly by operating it at a lower temperature. Silicon chips are being used in a multitude of applications in diverse thermal environments. It is very important to maintain the optimum working temperatures and keep thermal stresses on other supporting components to minimum. A printed wire board may contain heat generating components either flush or mounted on its surface. A successful thermal management can only be possible by designs that are based on detailed knowledge of heat transfer on and near these modules. Results presented in this paper will help in the design of electronic components and improve their performance. Some common applications include chip design for personal computers, laptops, signal processors, and workstations. More advanced applications may include integrated circuit design in supercomputer hardware, missile development, satellite, and space communication devices.

A comprehensive review of convection cooling options in electronic packages was provided by Incropera (1988). From this review he concluded a great need to study the effects related to the placement of discrete heat sources on a substrate and to explore the conjugate effects with three-dimensional flows. An experimental study of mixed convective transport from an isolated protruding heat source module mounted from a vertical surface was presented by Kang and Jaluria (1989). The effects of externally induced forced flow air cooling on the heat transfer rate from the heat source was investigated. The dependence of heat transfer rate and the temperature field on mixed convective parameter ($Gr/Re^{5/2}$) and on the module thickness was discussed.

Afrid and Zebib (1989) studied the effects of natural convection for air cooling of heated components on a vertical wall. Sathe and Joshi (1991) investigated the natural convection flow and heat transfer arising from a substrate mounted protruding heat source in a liquid filled enclosure. A parametric study to conjugate heat transfer from a substrate mounted protrusion in a square enclosure was reported by Sathe and Joshi (1992). Wroblewski and Joshi (1992) numerically investigated the transient start up, of a leadless chip carrier package mounted on a vertical substrate in a liquid filled cubic enclosure. They identified four stages of the transient to arrive at a steady natural convection flow. The substrate conduction was found to be important for the heat transfer process. Wroblewski and Joshi (1994) presented a three-dimensional computational study of steady natural convection cooling of a substrate-mounted protrusion in a rectangular enclosure filled with dielectric liquid. In a later study, Joshi et al. (1994) reported an experimental investigation of natural convection liquid immersion cooling of a three by three array of rectangular protrusions in an enclosure filled with dielectric liquid. Kim and Anand (1994) studied laminar developing flow over a series of parallel plates with surface mounted discrete heat sources. Flow and thermal characteristics and the effects of substrate conduction were studied numerically.

An experimental work for heated blocks in horizontal channels representing electronic circuit boards with heated chips was carried out by Herman et al. (1995). Two main flow regions: the bulk channel flow and the re-circulating flow were studied. A flow visualization study was carried out using the interferometry technique for a wide range of Reynolds numbers. Heindel et al. (1996) studied conjugate heat transfer in the board by coupling conduction in the solid and convection in the fluid. This problem involved natural convection from small heat sources mounted to a vertical wall inside a rectangular cavity. Thermal spreading across substrate provided an additional heat transfer mechanism. Gupta and Jaluria (1996) studied forced convection along an array of protruding heat sources in a rectangular channel. The influence of element spacing, channel height, and flow rates were examined. Choi and Kim (1996) studied the effects of conjugate heat transfer during mixed convection in a channel.

The above literature review indicates that fluid flow and heat transfer adjacent to protruding heat sources has been studied primarily for the limiting conditions of forced or natural convection. Gadepalli and Rahman (1996) studied the heat transfer from discrete heat sources on a vertical flat plate under cross-flow mixed convection. In their steady-state analysis, they studied the influence of important parameters such as Reynolds number, Richardson number, and the heat source spacing on the heat transfer rate. They found this influence to be stronger for laminar flow than for turbulent flow. Their study however was confined to a board with flush heat sources and for steady-state conditions. More recently, Raghavan and Rahman (1997) reported results for cross flow mixed convection near protruding heat sources on a circuit board. This study explored the effects of different geometric and flow parameters on conjugate heat transfer. However, this study was devoted only to the analysis of steady state heat transfer. From the survey of existing literature, it appeared that most experimental and analytical studies have been devoted to the investigation of steady state heat transfer in electronic circuit boards. A clear understanding of heat transfer mechanism during turning on or off of power in electronic equipment is still very inadequate in the open literature. Particularly, the development of mixed convective flow pattern around heat generating modules mounted on the board surface has not been investigated in any previous research work.

The physical geometry considered here is that of a flat conducting circuit board of finite thickness with discrete protruding heat sources on one surface of the board. The board is cooled at both the front and back surfaces by the combined influence of buoyancy induced flow in the vertical direction and a forced flow in the horizontal direction. A numerical model is developed to simulate the actual device considering heat generation in the components, conduction across the board, and convection to the fluid stream. The heat transfer characteristics during turning on of power is considered. The equations for the conservation of mass, momentum, and energy were solved in the fluid region. In the solid regions the velocity components were zero and the energy equation reduced to the transient heat conduction equation. Different dimensionless groups relevant to transient heat transfer in circuit boards under orthogonal mixed convection were identified. Calculations were carried out for mixed convection as well as for forced and natural convection limits to investigate

the velocity and temperature distributions and the local heat transfer rate.

2. Analysis and computation

The schematic of the physical problem is shown in the Fig. 1. A vertical board of finite length L, height H, and thickness b, is subjected to a horizontal fluid stream. The board has four heat sources mounted on its surface. Each of these sources are square in dimension with side l and height h_m, separated by a distance d_y and d_z in the y and z directions, respectively. The heat flux at the bottom of these mounted blocks is assumed to be uniform and has a value of q. The ambient fluid velocity and temperature are w_∞ and T_∞. It was assumed that the flow is laminar and incompressible. The variation of fluid properties was negligible over the temperature range encountered in the problem. The dimensionless groups defined in the nomenclature were used to express the governing transport equations in the dimensionless form. The resulting non-dimensional equations for the conservation of mass and momentum are:

$$\frac{\partial U}{\partial X}+\frac{\partial V}{\partial Y}+\frac{\partial W}{\partial Z}=0, \tag{1}$$

$$\frac{\partial U}{\partial \tau}+U\frac{\partial U}{\partial X}+V\frac{\partial U}{\partial Y}+W\frac{\partial U}{\partial Z} =\frac{1}{\mathrm{Re}}\left(\frac{\partial^2 U}{\partial X^2}+\frac{\partial^2 U}{\partial Y^2}+\frac{\partial^2 U}{\partial Z^2}\right), \tag{2}$$

$$\frac{\partial V}{\partial \tau}+U\frac{\partial V}{\partial X}+V\frac{\partial V}{\partial Y}+W\frac{\partial V}{\partial Z} =\frac{1}{\mathrm{Re}}\left(\frac{\partial^2 V}{\partial X^2}+\frac{\partial^2 V}{\partial Y^2}+\frac{\partial^2 V}{\partial Z^2}\right)+\mathrm{Ri}.\theta, \tag{3}$$

$$\frac{\partial W}{\partial \tau}+U\frac{\partial W}{\partial X}+V\frac{\partial W}{\partial Y}+W\frac{\partial W}{\partial Z} =\frac{1}{\mathrm{Re}}\left(\frac{\partial^2 W}{\partial X^2}+\frac{\partial^2 W}{\partial Y^2}+\frac{\partial^2 W}{\partial Z^2}\right). \tag{4}$$

The non-dimensional energy equations for the fluid and solid regions, respectively are:

$$\frac{1}{\mathrm{Re.Pr}}\frac{\partial \theta}{\partial \tau}+U\frac{\partial \theta}{\partial X}+V\frac{\partial \theta}{\partial Y}+W\frac{\partial \theta}{\partial Z} =\frac{1}{\mathrm{Re.Pr}}\left(\frac{\partial^2 \theta}{\partial X^2}+\frac{\partial^2 \theta}{\partial Y^2}+\frac{\partial^2 \theta}{\partial Z^2}\right), \tag{5}$$

$$\frac{\partial^2 \theta}{\partial X^2}+\frac{\partial^2 \theta}{\partial Y^2}+\frac{\partial^2 \theta}{\partial Z^2}=\left(\frac{\alpha_f}{\alpha}\right)\frac{\partial \theta}{\partial \tau}. \tag{6}$$

In Eq. (6), α is the solid thermal diffusivity, which corresponds to α_s in the board region and α_m in the mounted modules. The non-dimensional initial and boundary conditions are:

$$\tau\leqslant 0:\ U=0;\ V=0;\ W=0,\ \theta=0, \tag{7}$$

$$X=-B,\tau\geqslant 0:\ U=0,\ V=0,\ W=0,\ \theta_f=\theta_s,\quad \frac{\partial \theta_f}{\partial X}=\frac{k_s\partial\theta_s}{k_f\partial X}, \tag{8}$$

$$X=0,\ \tau\geqslant 0:\ U=0, V=0, W=0,$$

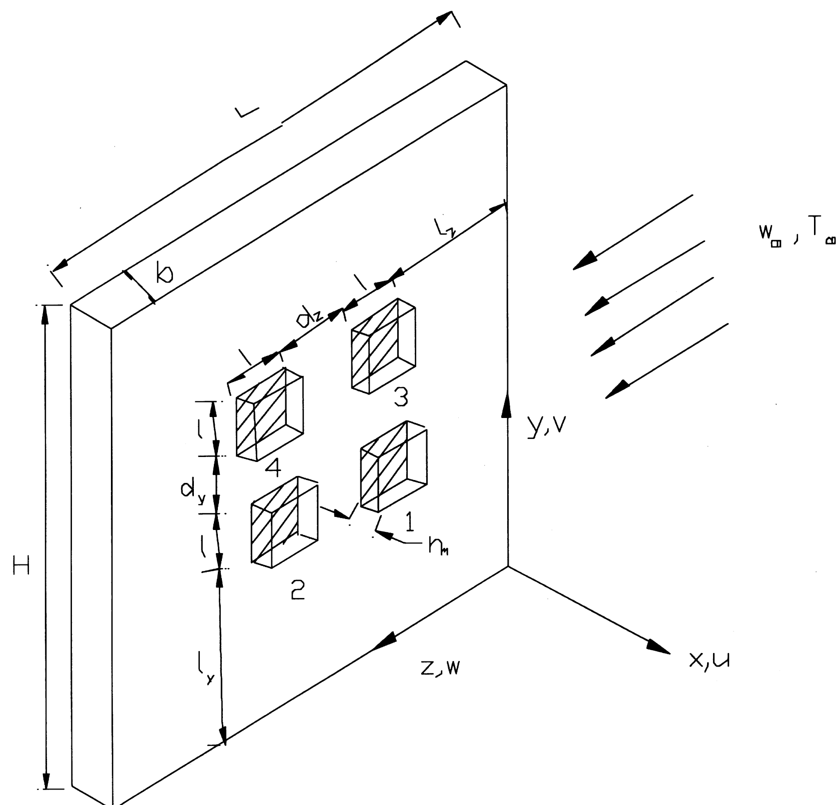

Fig. 1. Schematic diagram of the board with mounted heat sources.

$$-\frac{k_m \partial\theta_s}{k_f \partial X} = 1,\ L_Y < Y < L_Y + 1 \,\&\, L_Z < Z < L_Z + 1$$
$$= 1,\ L_Y < Y < L_Y + 1 \,\&\, L_Z + 1 + D_Z < Z < L_Z + 2 + D_Z = 1,\ L_Y + 1 + D_Y < Y < L_Y + 2 + D_Y \,\&\, L_Z < Z < L_Z + 1 = 1,$$
$$L_Y + 1 + D_Y < Y < L_Y + 2 + D_Y \,\&\, L_Z + 1 + D_Z < Z < L_Z + 2 + D_Z$$
$$= 0,\ \text{elsewhere.} \tag{9}$$

$$X \to -\infty,\ X \to \infty,\ \text{and}\ \tau \geqslant 0: \quad V = 0,\ W = 1,\ \theta = 0, \tag{10}$$

$$Y = 0\ \text{and}\ \tau \geqslant 0: V = 0,\ W = 1,\ \theta = 0, \tag{11}$$

$$Z = 0\ \text{and}\ \tau \geqslant 0: V = 0,\ W = 1,\ \theta = 0. \tag{12}$$

The non-dimensional form of boundary conditions at different surfaces of the protruding modules are:

At $X = H_M, L_Y < Y < L_Y + 1 \& L_Z < Z < L_Z + 1$
and $X = H_M, L_Y < Y < L_Y + 1 \& L_Z + 1 + D_Z < Z < L_Z + 2 + D_Z$
and $X = H_M, L_Y + 1 + D_Y < Y < L_Y + 2 + D_Y \& L_Z < Z < L_Z + 1$
and $X = H_M, L_Y + 1 + D_Y < Y < L_Y + 2 + D_Y \& L_Z + 1 + D_Z < Z < L_Z + 2 + D_Z$

$$U = 0,\ V = 0,\ W = 0,\ \theta_f = \theta_m, \quad \frac{\partial\theta_f}{\partial X} = \frac{k_m}{k_f}\frac{\partial\theta_m}{\partial X}. \tag{13}$$

At $0 < X < H_M,\ Y = L_Y \& L_Z < Z < L_Z + 1$
and $0 < X < H_M, Y = L_Y \& L_Z + 1 + D_Z < Z < L_Z + 2 + D_Z$
and $0 < X < H_M, Y = L_Y + 1 + D_Y \& L_Z < Z < L_Z + 1$
and $0 < X < H_M, Y = L_Y + 1 + D_Y \& L_Z + 1 + D_Z < Z < L_Z + 2 + D_Z$
and $0 < X < H_M, Y = L_Y + 1 \& L_Z < Z < L_Z + 1$
and $0 < X < H_M, Y = L_Y + 1 \& L_Z + 1 + D_Z < Z < L_Z + 2 + D_Z$
and $0 < X < H_M, Y = L_Y + 2 + D_Y \& L_Z < Z < L_Z + 1$
and $0 < X < H_M, Y = L_Y + 2 + D_Y \& L_Z + 1 + D_Z < Z < L_Z + 2 + D_Z$

$$U = 0,\ V = 0,\ W = 0,\ \theta_f = \theta_m, \quad \frac{\partial\theta_f}{\partial Y} = \frac{k_m}{k_f}\frac{\partial\theta_m}{\partial Y}. \tag{14}$$

At $0 < X < H_M, L_Y < Y < L_Y + 1 \& Z = L_Z$
and $0 < X < H_M, L_Y < Y < L_Y + 1 \& Z = L_Z + 1 + D_Z$
and $0 < X < H_M, L_Y + 1 + D_Y < Y < L_Y + 2 + D_Y \& Z = L_Z$
and $0 < X < H_M, L_Y + 1 + D_Y < Y < L_Y + 2 + D_Y\ Z = L_Z + 1 + D_Z$
and $0 < X < H_M, L_Y < Y < L_Y + 1 \& Z = L_Z + 1$
and $0 < X < H_M, L_Y < Y < L_Y + 1 \& Z = L_Z + 2 + D_Z$
and $0 < X < H_M, L_Y + 1 + D_Y < Y < L_Y + 2 + D_Y \& Z = L_Z + 1$
and $0 < X < H_M, L_Y + 1 + D_Y < Y < L_Y + 2 + D_Y \& Z = L_Z + 2 + D_Z$

$$U = 0,\ V = 0,\ W = 0,\ \theta_f = \theta_m, \quad \frac{\partial\theta_f}{\partial Z} = \frac{k_m}{k_f}\frac{\partial\theta_m}{\partial Z}. \tag{15}$$

At the two outflow boundaries ($y = H$ and $z = L$), the transport was assumed to be locally parabolic, i.e., gradients of velocity and temperature were assumed to be approximately zero. From the above mentioned mathematical model, it can be seen that the factors that might influence the flow and heat transfer characteristics are: the Reynolds number, the Richardson number, the Fourier number, distances of sources from natural and forced convection leading edges, source spacings in the vertical and horizontal directions, board thickness, and the solid-to-fluid thermal conductivity ratios.

The governing transport equations along with the boundary and initial conditions listed above were solved using a Cartesian grid structure covering the entire domain of interest (both solid as well as fluid regions). The extent of the computation domain perpendicular to the plate was determined

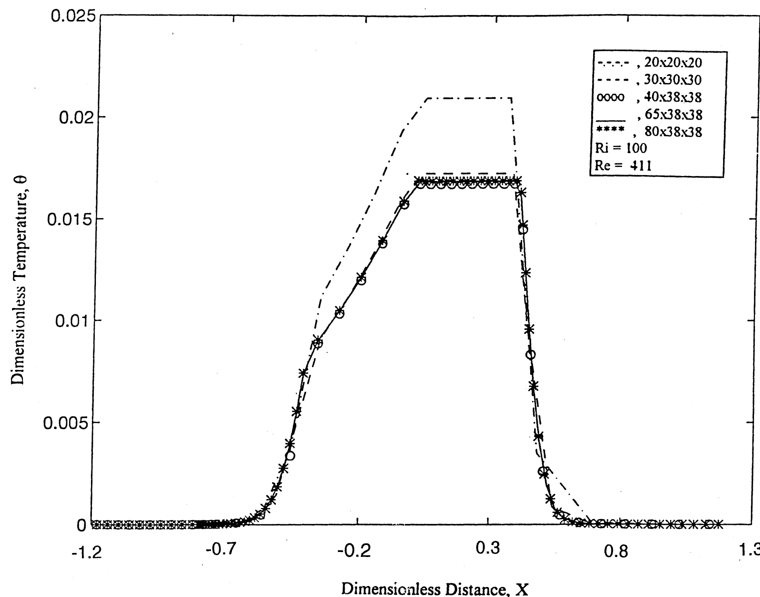

Fig. 2. Temperature profile at heat source 1 ($Y = 8.5, Z = 8.5$) for different grid distributions.

from a series of trial runs to adequately capture the velocity and thermal boundary layers for all Richardson numbers considered in this investigation. The finite volume equations were derived using the principles of conservation of mass, momentum, and energy at each cell. The hybrid difference scheme was used to determine the relative contribution of convection and diffusion to a cell from its neighbors in terms of cell Peclet number. The variables were stored in a staggered fashion for cell conservation and for each cell the velocity components were stored at downstream boundaries, whereas pressure and temperature were stored at cell centers. The harmonic mean of thermal conductivities was used to calculate heat transfer at the solid–solid and solid–fluid interfaces. The discretized equations were solved using the SIMPLEST algorithm developed by Spalding (1980). The iterative solution was continued until the residuals for all computational cells became negligible (less than 10^{-7}) and the velocity components and temperature values did not change from one iteration to the next. All equations had to be solved simultaneously because of the coupling between velocity and temperature through the buoyancy term.

The grid structure for computation was optimized by performing a systematic grid independence study. The grid structure was non-uniform in nature and distributed over the fluid and solid regions to adequately capture steep velocity, pressure, and temperature gradients due to the presence of heat sources. Grid nodes were finely spaced near the solid–fluid interfaces where field variables changed rapidly with distance and coarsely farther away from the plate. The model was quite sensitive to changes in grid size in the x direction. Fig. 2 shows the results of the grid independence study. The temperature profile at one of the heat sources is shown. It can be seen that the temperature profile was practically identical for $40 \times 38 \times 38$ mesh and a denser $65 \times 38 \times 38$ mesh; but showed some differences for lower number of grids. A mesh containing $65 \times 38 \times 38$ cells in the x,y, and z directions was chosen for the numerical simulation. Since the present numerical scheme used an iterative solution procedure, it was also essential to check the number of sweeps (iterations over the entire computational domain) required to arrive at a converged solution. A series of runs with different sweep numbers were made. It was found that 900 sweeps would be sufficient to provide accurate numerical results. A time step optimization procedure was carried out to determine the optimum time step required for the transient simulation. Unlike the grid size, the temperature distribution plot did not show any significant variation with the choice of time step. A time step of $d\tau = 1$ was chosen for the numerical simulation.

3. Results and discussion

The mathematical model developed in the last section was used to investigate the mutual interaction of heat sources on a circuit board when subjected to a cross flow and transient thermal loading. The number of heat sources and the rate of heat generation vary according to the type of application. The board used here is of finite thickness and heat transfer from the back of the board was also accounted for. The exact location of the heat sources are shown in Fig. 1. In order to calculate dimensionless parameters for numerical computation, air at atmospheric pressure and temperature (1 atm and 20°C) was taken as the fluid medium, masonite ($k_s = 0.14$ W/mK) as the board material, and copper ($k_m = 381$ W/mK) as the material of the protruding module. This choice of materials is one of the several combinations that could be used. Dielectric liquids are used in immersion cooling applications. Moreover, the printed circuit boards frequently use composite materials. These materials are non-homogeneous and anisotropic. In that situation, conduction within the board has to be modeled by accounting for these effects. A Reynolds number of 411, calculated using the size of heat sources ($l = 0.0254$ m) as the length scale, was used in all numerical simulations. This provided a laminar flow over the entire surface of the board. The rate of heat generation was assumed to be constant for this study. In addition, the numerical computation used $L_y = L_z = 8$, $D_y = D_z = 1$, $B = 0.4$, and $H_M = 0.4$. The computation domain extended to $H = 19$ in the vertical direction and $L = 19$ in the horizontal direction. These downstream distances after the heat sources were found to be adequate to justify local parabolic assumption at the exit boundaries. Further enlargement of the downstream distances did not have any effect on the temperature distribution at the heat sources. The local heat transfer coefficient at the solid–fluid interface was calculated by using local heat flux and interfacial temperature. These quantities were calculated using temperatures of the solid and the fluid cells adjacent to the interface and satisfying a local energy balance. The average heat transfer coefficient was taken as the mean of the local coefficients.

The type of transient considered here is starting of heating within an uniform forced flow in the system, corresponding to switching on of power in an electronic equipment. The Richardson number determines the relative magnitude of natural and forced convection processes. Thus a low Ri value corresponds to a forced convection dominated process, while a high value corresponds to a buoyancy dominated flow. The results of this study will show the interaction between mounted circuit modules and their influence on velocity field adjacent to the board, and in particular, around the heated modules.

Table 1
Transient Nusselt number at mounted heat sources

Richardson number (Ri)	Dimensionless time (τ)	Heat source 1	Heat source 2	Heat source 3	Heat source 4
2.5	4	11.0346	10.5687	10.8693	9.7416
	16	11.1186	9.6771	10.9063	7.9958
	70	10.9122	8.8634	10.5552	6.9204
	100	10.8732	8.7510	10.5072	6.7752
100	4	15.5431	19.3094	14.8547	15.5083
	16	15.9400	19.2847	14.6082	15.4621
	70	16.0124	19.0688	14.5511	15.2151
	100	16.0140	19.0503	14.5476	15.1953
1000	4	26.8423	25.5942	24.4297	25.2938
	16	26.8948	25.6023	24.0761	24.7606
	70	28.8974	25.6704	23.9772	24.6673
	100	26.8983	25.6714	23.9735	24.6595

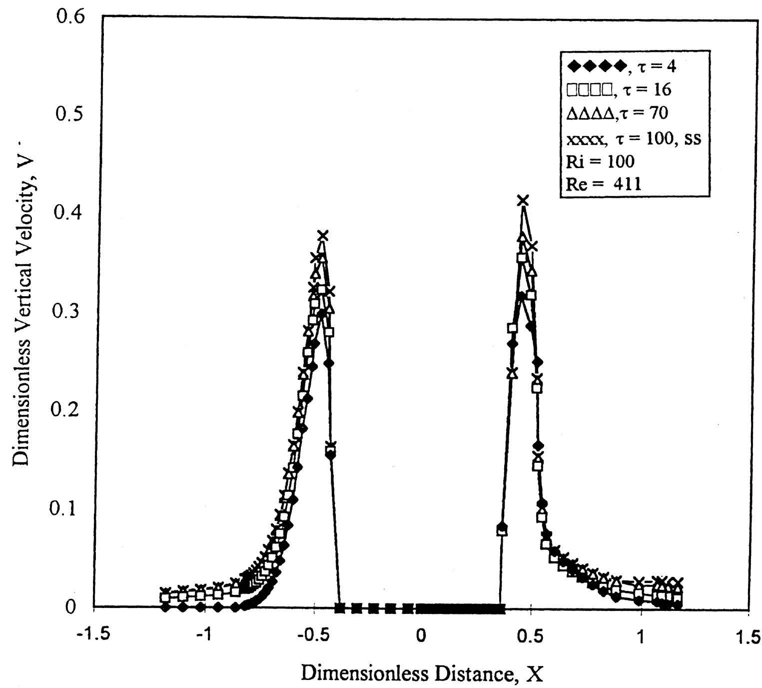

Fig. 3. Vertical velocity variation at heat source 1 ($Y = 8.5, Z = 8.5$).

The transient variation of Nusselt number at four heat source locations is presented in Table 1 for three different Richardson numbers ranging from the natural to the forced convection limit. From a series of computer runs with different values of Richardson number and by observing the flow patterns adjacent to the heated modules (Raghavan, 1997), it was found that the flow is forced convection dominated when $\mathrm{Ri} \leqslant 2.5$ and natural convection dominated when $\mathrm{Ri} \geqslant 1000$. For any given forced flow velocity, the effects of buoyancy increases with Richardson number. At $\mathrm{Ri} \leqslant 2.5$, the fluid particles moves predominantly in the forced flow direction. The vertical motion due to buoyancy are limited in the stagnant regions between sources 1 and 2, and between sources 3 and 4. At $\mathrm{Ri} \geqslant 1000$, the fluid particles that have approached the heat sources are heated up quickly and moves upward essentially forming a vertical plume. In between these limits the flow is mixed convective in nature with varying influence of each mechanism based on the value of the Richardson number.

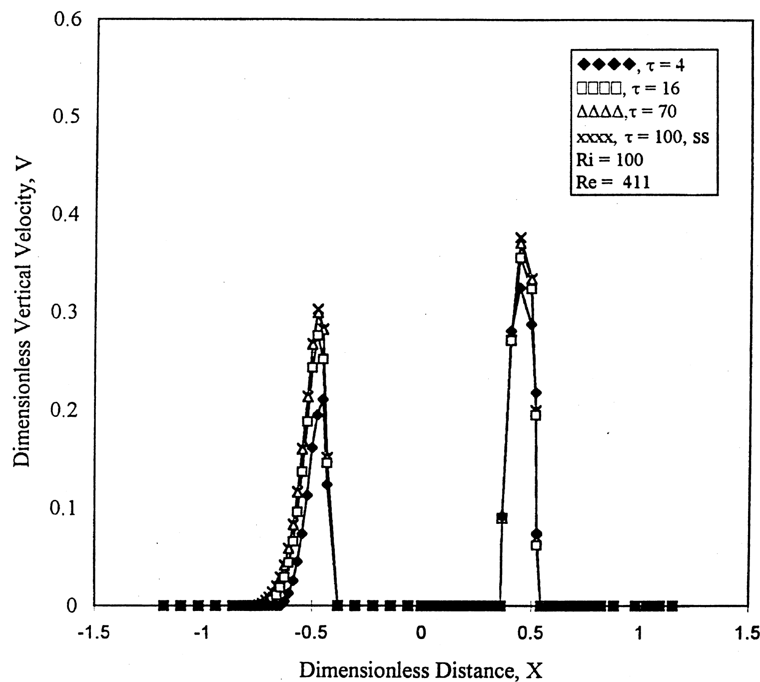

Fig. 4. Vertical velocity variation at heat source 2 ($Y = 8.5, Z = 10.5$).

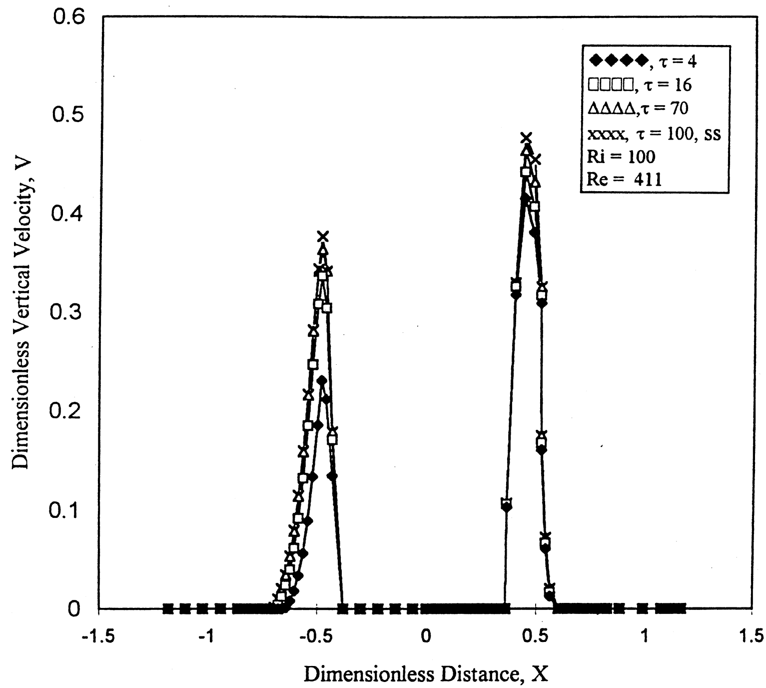

Fig. 5. Vertical velocity variation at heat source 3 ($Y = 10.5, Z = 8.5$).

As the power is turned on, the effects of buoyancy increases with time. The flow structure around the heat sources changes accordingly and reaches the steady-state pattern within $\tau = 100$. The Nusselt numbers change with time till they reach a steady state condition. The values of the Nusselt numbers are representative of the heater temperatures at different stages of the transient. Higher the Nusselt number value, better the heat transfer rate and cooler the heater surface temperature. It can be noticed that at most conditions the Nusselt number is larger at smaller values of τ and gradually decreases with time to approach the final steady-state condition. This trend is because the thermal boundary layer thickness increases with increase in time.

For $\mathrm{Ri} = 2.5$, the flow is predominantly forced convection. The two heat sources closest to the forced convection leading edge, sources 1 and 3, have the higher rate of heat transfer meaning higher Nusselt numbers and lower surface temperatures as compared to the sources 2 and 4. The changes seen

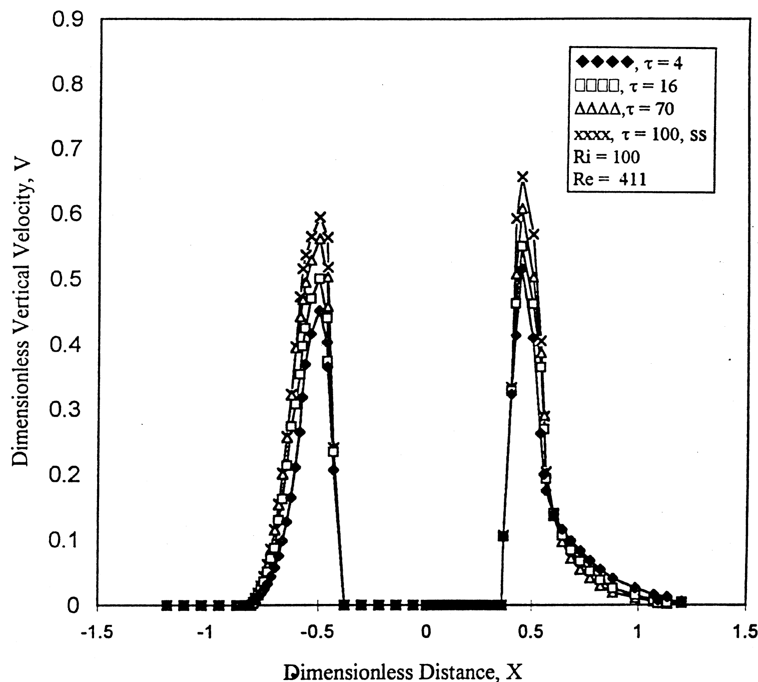

Fig. 6. Vertical velocity variation at heat source 4 ($Y = 10.5, Z = 10.5$).

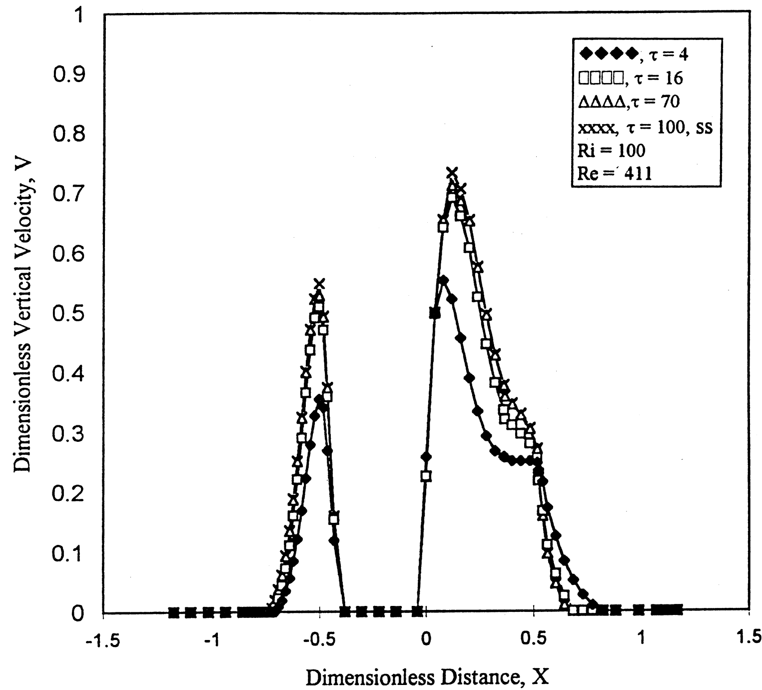

Fig. 7. Vertical velocity variation at an unheated location between the sources ($Y = 9.5, Z = 9.5$).

in heat sources 2 and 4 are much higher and more rapid than for sources 1 and 3. This shows relatively higher heat transfer activity near these sources. Ri = 100 corresponds to a truly mixed convection flow regime. Increasing Ri for a constant Re implies higher buoyancy forces for the same rate of forced convection. Hence, the Nusselt numbers increase with increase in Ri. For Ri = 1000, the flow is buoyancy dominated. It can be seen that Nusselt numbers have increased significantly in magnitude for all four heat sources. The two heat sources closest to the natural convection leading edge, sources 1 and 2, have higher Nusselt numbers when the steady-state condition is reached. At the start of the transient, heat sources 1 and 2 show better cooling trends than the other heat sources and heat sources 3 remains the hottest heat source until the steady-state condition is reached.

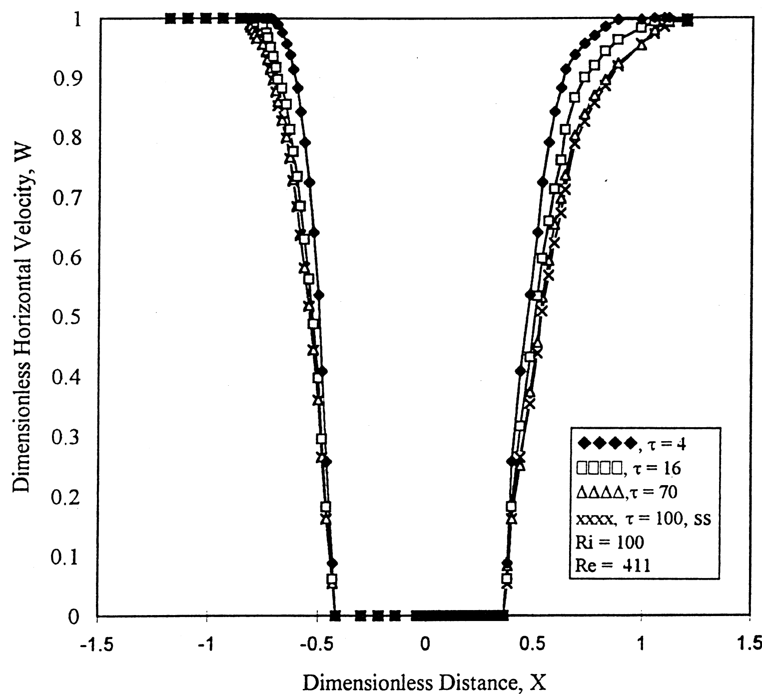

Fig. 8. Horizontal velocity variation at heat source 1 ($Y = 8.5, Z = 8.5$).

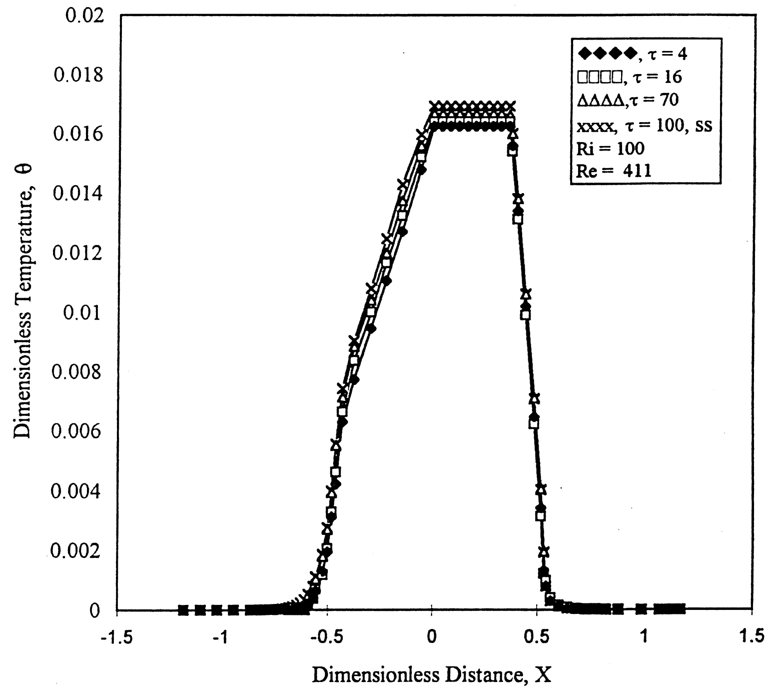

Fig. 9. Temperature variation at heat source 1 ($Y = 8.5, Z = 8.5$).

Figs. 3–7 show the variation of vertical velocity adjacent to both sides of the board and the modules at different time intervals. The profiles show variation at the four heat sources and at an unheated location between the heat sources. A Richardson number of 100 was used for these calculations. It can be noticed that the curves to the right have a slightly higher peak velocities due to the presence of heat sources on that side of the board. Otherwise profiles are almost similar on both sides. As soon as power is turned on, the board and module temperatures increase over the initial ambient temperature and buoyancy induced flow starts to develop. At each heat source location (Figs. 3–6) and at other location swept by hot fluid (Fig. 7) it can be noticed that the vertical velocity starts from a zero initial condition and gradually increases with time. The velocities are zero through the board and the mounted modules. The thickness of the boundary layer in-

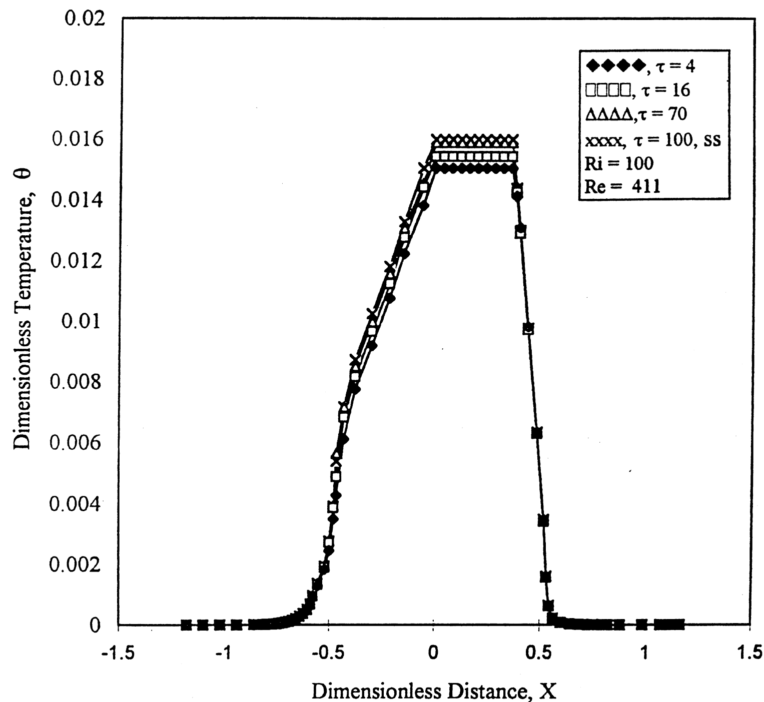

Fig. 10. Temperature variation at heat source 2 ($Y = 8.5, Z = 10.5$).

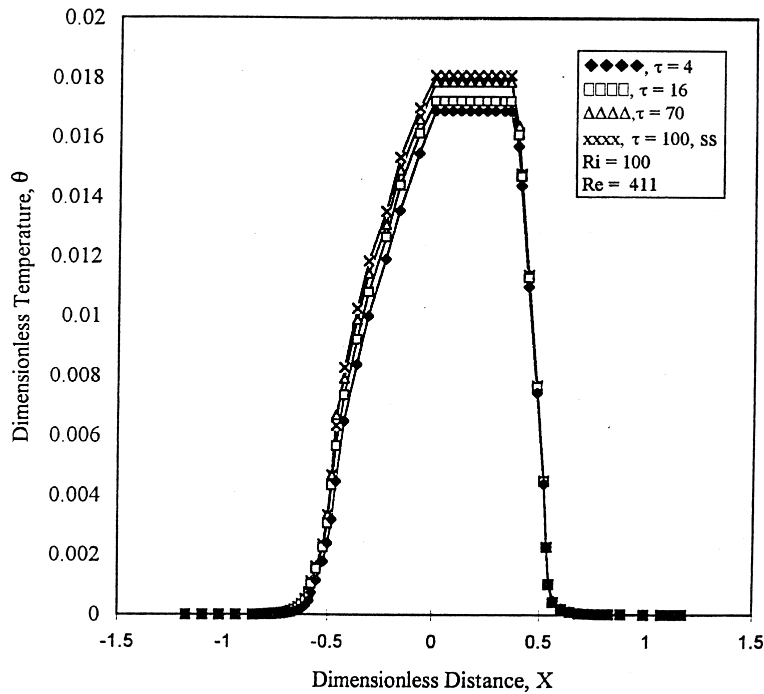

Fig. 11. Temperature variation at heat source 3 ($Y = 10.5, Z = 8.5$).

creases with time. The velocity increases with increase in vertical height (Y) owing to the development of buoyancy induced flow in that direction. Results corresponding to four different time intervals have been plotted here. Beyond $\tau = 100$, there was no further change of velocity at any location on the board confirming that a steady-state condition has been reached for the entire computational domain. Fig. 8 shows the horizontal velocity distribution in the boundary layers adjacent to the surface of the board and the mounted modules. The velocity at the surface of the board and on top of the modules is zero and we see a gradual decrease from the free stream velocity to zero on either side of the board. During the transient, horizontal velocity decreases in magnitude until a steady-state condition is reached.

Figs. 9–12 show the temperature distribution in the boundary layers on the back side of the board surface and in front of the mounted modules. On either side of the board the temperature decreases monotonically to its free stream value at

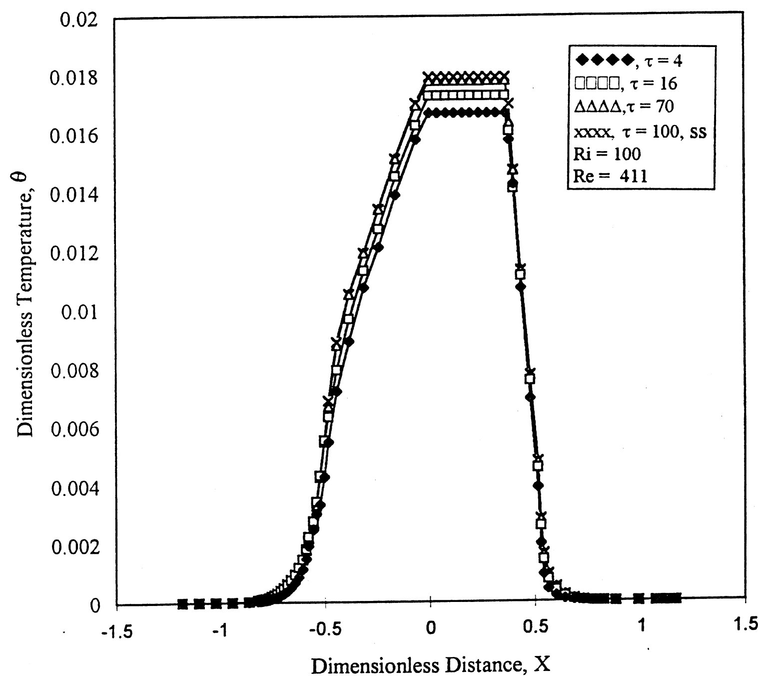

Fig. 12. Temperature variation at heat source 4 ($Y = 10.5, Z = 10.5$).

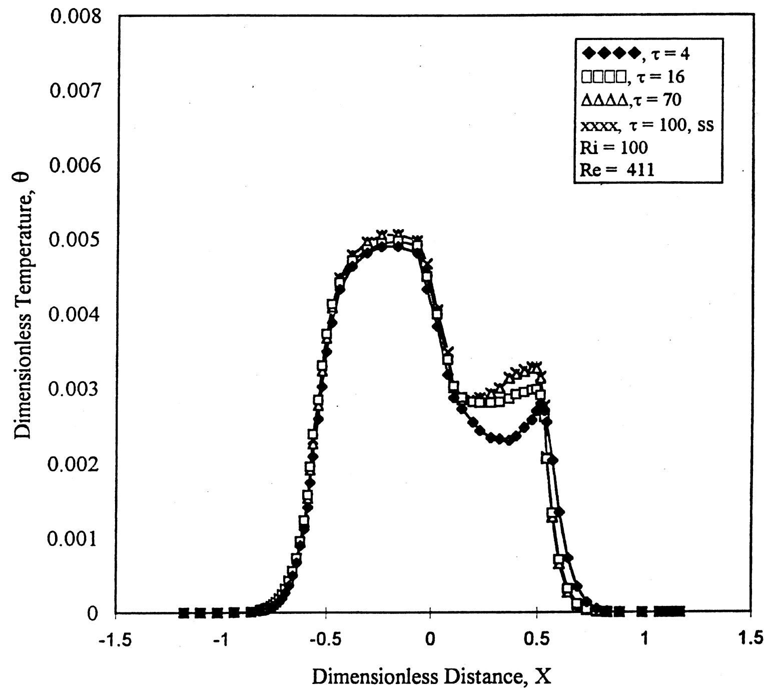

Fig. 13. Temperature variation at an unheated location between the sources ($Y = 9.5, Z = 9.5$).

all locations. The temperatures of sources 1 and 2 are somewhat lower than sources 3 and 4. The temperature in the solid region varies linearly as expected. The temperature reaches steady-state faster than the velocity as seen from the temperature profiles at different time intervals. The temperature at the center of the board presented in Fig. 13, shows an interesting profile. The temperature of the fluid drops adjacent to the board surface but then increases due to the hot fluid circulation shown by the peaks on the right side of the plot. As time increases the temperature of the fluid increases and a smoother peak is seen at the steady-state condition. The conduction across the board is strong but conduction in the y and z directions are rather small. The temperature gradient at the solid–fluid interfaces can be used to calculate the rate of heat transfer from the front and back sides of the board. It was found that approximately 75% heat dissipation takes place from the surfaces of the mounted modules and from the front surface of the board, whereas 25% energy is conducted through the board and dissipated from the back surface. This study provided an insight into the mutual interaction of the heated modules and their behavior with time during turning on of power in an electronic equipment in the presence of a horizontal fluid stream. This information will be useful in the thermal design of electronic equipment.

4. Conclusions

The transient response of discrete heat sources on a conducting board of finite thickness in the presence of cross-flow mixed convection is presented. The variation of Nusselt number with Fourier number was explored. The Nusselt number was found to be a strong function of Richardson number. An explicit variation of velocity and temperature was studied over a period of time until a steady-state condition was reached. The temperature profile developed faster than the velocity on both sides of the board. The heat transfer from both sides of the board were found to be significant during the entire transient period. Approximately 75% heat dissipation occurred at the front surface and mounted modules, whereas 25% of energy was transmitted through the board and dissipated from the back surface.

References

Afrid, M., Zebib, M., 1989. Natural convection of air cooling of heated components mounted on a vertical wall. Numerical Heat Transfer Part A 15, 243–259.

Choi, C.Y., Kim, S.J., 1996. Conjugate mixed convection in a channel: modified five percent deviation rule. International Journal of Heat and Mass Transfer 39, 1233–1234.

Gadepalli, P., Rahman, M.M., 1996. Conjugate heat transfer in electronic equipment. Proceedings of the ASME Heat Transfer Division, vol. 2, HTD-333, 219–229.

Gupta, A., Jaluria, Y., 1996. Forced convective liquid cooling of arrays of protruding heated elements mounted in a rectangular duct. Proceedings of ASME Heat Transfer Division vol. 2, HTD-333, 187–209.

Heindel, T.J., Ramadhyani, S., Incropera, F.P., 1996. Conjugate natural convection from an array of protruding heat sources. Numerical Heat Transfer Part A 29, 1–18.

Herman, C., Kang, E., Haung, H., Purnaik, B., 1995. Experimental visualization of unsteady temperature fields in electronic cooling applications. Cooling and Thermal Design of Electronic Systems ASME HTD-319, 33–40.

Incropera, F.P., 1988. Convection heat transfer in electronic equipment cooling. Journal of Heat Transfer 110, 1097–1111.

Joshi, Y., Kelleher, M.D., Powell, M., Torres, E.I., 1994. Natural convection heat transfer from an array of rectangular protrusions in an enclosure filled with dielectric liquid. Journal of Heat Transfer 116, 138–147.

Kang, B.H., Jaluria, Y., 1989. Mixed convection transport from a protruding heat source module on a vertical surface. AIAA Journal of Thermophysics and Heat Transfer 4, 384–390.

Kim, S.H., Anand, N.K., 1994. Laminar developing flow and heat transfer between a series of parallel plates with surface mounted

discrete heat sources. International Journal of Heat and Mass Transfer 37, 2231–2244.

Raghavan, J., 1997. Numerical computation of steady and transient heat transfer near flush and mounted heat sources on a circuit board. M.S. Thesis, University of South Florida, May, 1997.

Raghavan, J., Rahman, M.M., 1997. Analysis of mixed convective cross flow near protruding heat sources on a vertical circuit board. Proc. ASME Heat Transfer Division HTD-351, 337–346.

Sathe, S.B., Joshi, Y., 1991. Natural convection arising from a heat generating substrate mounted protrusion in a liquid filled two-dimensional enclosure. International Journal of Heat and Mass Transfer 34, 2149–2163.

Sathe, S.B., Joshi, Y., 1992. Natural convection liquid cooling of a substrate-mounted protrusion in a square enclosure: a parametric study. Journal of Heat Transfer 114, 401–409.

Spalding, D.B., 1980. Mathematical modeling of fluid mechanics, heat transfer, and chemical reaction processes. A Lecture Course, CFDU Report, HTS/80/1, Imperial College, London.

Wroblewski, D.E., Joshi, Y., 1992. Transient natural convection from a leadless chip carrier in a liquid filled enclosure: a numerical study. Advances in Electronic Packaging ASME/EEP-1, 235–248.

Wroblewski, D.E., Joshi, Y., 1994. Liquid immersion cooling of a substrate-mounted protrusion in a three-dimensional enclosure: the effects of geometry and boundary conditions. Journal of Heat Transfer 116, 112–119.